Princeton University Department of Mechanical and Aerospace Engineering

Horus: An Origami-Unfolding Solar Array

Santiago Aguirre, Joshua Freeman, Colin Reilly,
Benjamin Shi, Maxwell Schwegman

February 20, 2018

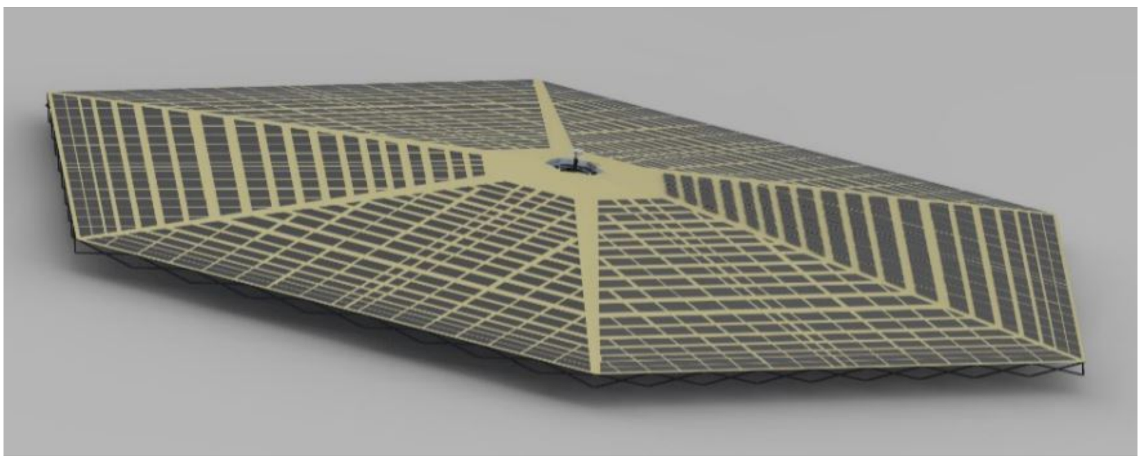

Fully deployed Horus CAD model.

Advisors: Prof. Luis Gonzalez, Prof. Andrej Kosmrlj, Prof. Barry Rand, Prof. Jeremy Kasdin

1 Introduction

While colonizing Mars might only be a dream today, NASA has put ambitious goals in place to send humans to Mars in the 2030s. Such missions will drastically increase a need for power production on Mars's surface. Low air density and no liquid water on the surface make solar power generation perhaps Mars's most viable option for power production. To even arrive at Mars, a Martian solar power system must be lightweight and pack a large area of solar panels into a small volume for transport. Once there, the system must be able to unpack autonomously over rough terrain and hold the solar panels off the ground in its deployed state. It must endure a harsh Martian operating environment, consisting of wind speeds of up to 50 m/s, daily temperature fluctuations of over 100° C, and a constant accumulation of obscuring dust. As a response to these challenges, we propose the Horus - an autonomously deploying, origami-unfolding solar array.

The Horus uses an expanding ring structure to unfold a solar membrane, exposing 1,061 m^2 of solar panels to Martian sunlight and producing an average of 130 kW per year on the equator, with a maximum 155kW at perihelion and a minimum of 103 kW at aphelion. The solar panels rest on a foldable membrane that, including all structural elements, packs into a volume of 10 m^3; the entire payload weighs approximately 1,390 kg. The membrane consists of an electrodynamic dust screen (EDS) system to mitigate dust accumulation and an axially symmetric array of photovoltaic (PV) cells mounted on a Kevlar membrane sized to support the design loads. Each of the six triangular segments of the hexagonal solar membrane are independently wired and configured to ensure continued power production in the event of the failure of any segment, while an innovative dust mitigation system repels dust particles away from Horus's solar panels to ensure continued maximum power production. These qualities make Horus a simple but effective means of generating power for future manned missions on Mars.

2 Origami Packaging

To achieve a high ratio between deployed area and packed volume, Horus folds the membrane of solar panels into a hexagonal tube following a pattern known as the Flasher model.[1] This ratio can be tuned to any desired value by altering the complexity of the Flasher, provided the membrane material is suitably thin. In Figure 2.1 below, each black line represents a fold in the pattern; these folds divide the sheet into a mosaic of triangular and rectangular regions where solar panels are placed. The complexity of the Flasher is set by three parameters. The first parameter, denoted m, is the number of the sides of the polygon that the pattern will wrap around. For the hexagonal versions of the Flasher shown in Figure 2.1, $m = 6$. The second parameter, h, is equal to the number of solar panel regions in each triangular section highlighted in Figure 2.1c. This parameter relates to H, the height of the packed membrane, by the formula $H = \frac{h}{\sqrt{3}}L$, where L is the side length of the polygon the membrane folds into. $h = 4$ for the model in Figure 2.1d, meaning that the height of the Horus in its packed state will be $H = \frac{4}{\sqrt{3}}L$. Finally, the parameter r is the number of triangular regions that must be lined up to go from the central polygon to the edge of the membrane. With $m = 6$, $h = 4$, $r = 4$, and L set to 1.1 m, the membrane of the Horus would have a total unfolded area of 1,076 m^2. The versions of the Flasher shown in Figure 2.1c and 2.1d will only pack perfectly if the material being folded is infinitely thin. To enable the solar membrane to pack properly, 1 cm wide gaps in the solar panels, illustrated in Figure 3.1, must be placed at the fold lines. These gaps reduce the area that can be used to collect solar power by about 15 m^2 to give the Horus a PV area of 1,061 m^2. The volume of space inside the membrane's packed hexagonal tube state, approximately 8 m^3, can be obtained by multiplying the area of the central hexagon by H. Given a membrane thickness of 0.272 mm, such as that in Figure 3.1, the thickness of the packed hexagonal prism would be 2.3 cm, rounded up to 3 cm to account for imperfections in the packing process. The 10 m^3 volume of the Horus can be computed by adding an additional thickness of 8 cm around the outside of the packed membrane to account for the space taken by the support structure.

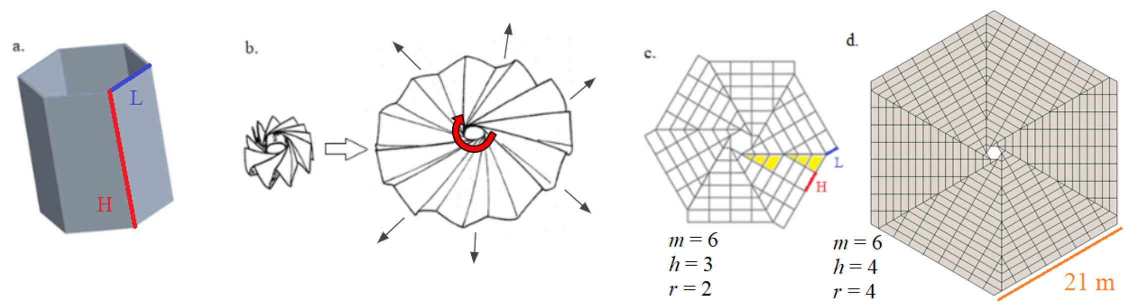

Figure 2.1: The Flasher fold configuration. (a) Flasher pattern with $m = 6$ in stowed configuration. (b) Left to Right: deployment of the Flasher membrane. Notice the combination of radial force and rotation of the core.[2] (c) Fully expanded example of the Flasher model. Two triangles with three sections apiece reach from the center of the pattern to the perimeter. (d) Variant of The Flasher used for the Horus.

3 Membrane Design and Performance

The thickness of the Horus's membrane comes from three main subsystems stacked on top of each other: an EDS system for dust mitigation, a photovoltaic array for power generation, and the Kevlar structural substrate.

Material	Density, $\frac{kg}{m^3}$	Mass, kg
Kevlar	1440	123.95
Supreme 10HT	1370	110.47
$GaAs$	2650	5.32
SIO_2	6800	265
ITO	2430	68
SCHOTT Glass	5320	12.15

Table 3.1: Mass and Density of Membrane Materials

The total mass of the membrane is 584.89 Kg. This translates to 2,170 N on Mars or 5,737 N on Earth.

3.1 System 1: Kevlar Support and Epoxy Attachment Layers

Kevlar KM2 was selected as the primary support layer for the membrane due to its low weight, high tensile strength, and desirable thermal properties. Kevlar KM2 has been a valuable material for the development of space shields designed to protect the International Space Station from debris due to its high resistance to ballistic impacts and thermal cycling in space, making it a trustworthy material for the support layer.[3]

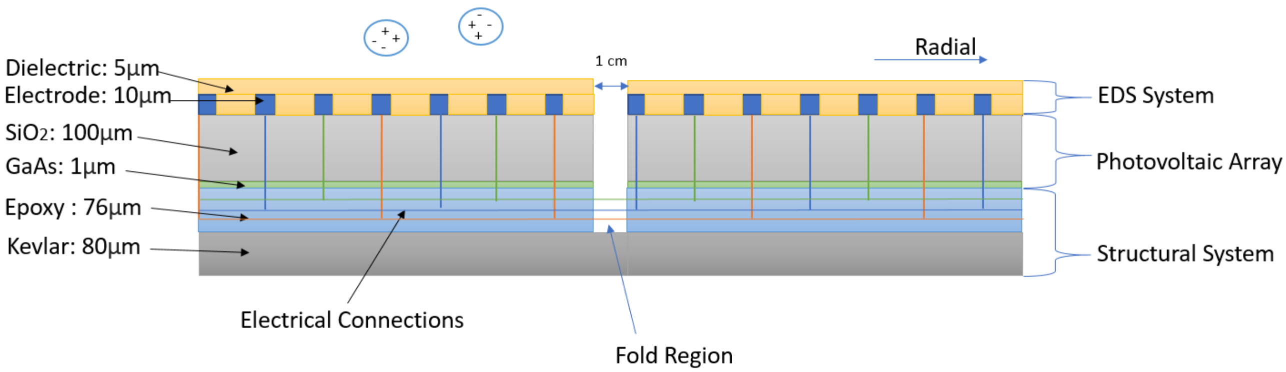

Figure 3.1: Membrane cross section. The total thickness of the membrane is 272 μm. Note the electrical connections (designated as blue, red and green lines) running through the epoxy and powering each individual electrode. Electrode quantity/size not drawn to scale.

Attaching the solar panel assembly to the support layer poses a challenge, as the PV and dust mitigation assembly is too thin to reliably use metal supports, bolts, or clamps. Instead, the solar panels will be bonded with a single-compound epoxy to the Kevlar membrane. Supreme 10HT was chosen because of its insulating properties and a wide temperature service range of 4K to 373K over many cycles. In addition, Supreme 10HT's mechanical properties become more favorable at lower temperatures since its tensile and shear modulus are inversely proportional to temperature.[4]

An 80 μm layer of Kevlar KM2 cloth will ensure the that the panels are properly supported and that the structure does not collapse under its own weight. Once fully deployed, the cloth will be under tension to limit sagging. The mechanical properties of Kevlar were extracted from Dupont's brochure[5] and its ultimate tensile strength was obtained from a joint study between The U.S. Army Research Laboratory at Aberdeen Proving Grounds and the University of Arizona.[6] The mechanical properties of Supreme 10HT were extracted from a material data sheet provided by Master Bond, the manufacturers of Supreme 10HT.

3.2 System 2: Photovoltaic Array

Current power requirements for a Martian surface mission are approximately 40 kW at all times. This means that Horus must generate an average of 960 kWh per sol, much of which must be stored by batteries in order to power operations at night time. In order to meet these specifications, Horus utilizes thin film Gallium Arsenide (GaAs) solar cells. GaAs solar cells have been used in space applications for multiple missions, including the Spirit and Opportunity rovers, as well as the Mars Phoenix Lander,[7] due to their high efficiency and radiation resistance compared to conventional silicon solar cells.[8] These features are desirable because Mars receives around 40% of the solar radiation that Earth does and lacks a radiation resistant magnetic field.[9] Thin film single junction GaAs solar cells developed by Alta Devices will minimize the thickness of the solar array while providing an efficiency of 28.8%.[10] These solar cells also function ideally in cold conditions, with their power output increasing by .09% for every degree Celsius below 25°. By using previous temperature data collected, change in power output due to temperature was estimated.[11] Utilizing forecasted solar fluxes on Mars starting in 2034 in conjunction with estimated peak solar hours, the average power and energy outputs of Horus can be calculated.[12] The peak solar hours, a value necessary to solve for the amount of kilowatt-hours Horus can produce, were estimated by taking the peak solar hour of an analogous position on Earth and adjusting that value from the rate of Earth's rotation to the rate of Mars's rotation. In Table 3.2 are the calculated energy outputs of Horus along the equator, on the 30° South latitude line, and on the 50° North latitude line, all of which are locations of interest for human missions to Mars. All calculated energy-production values have taken solar irradiation, temperature, optical transmission through the EDS system, and electrical losses due to resistive heating of the wiring into account.

Table 3.2: Yearly and seasonal energy output of Horus at varying latitudes.

Location	Peak Solar Hours	Average Yearly Output(kWh/sol)	Average Winter Output(kWh/sol)	Average Summer Output(kWh/sol)
Equator	9.8	1293.78	1127.45	1475.96
30°South	6.1	687.55	453.58	941.99
50°North	3.4	263.91	350.40	172.87

3.2.1 The Impact of Martian Dust

Dust on Mars will affect the power output of Horus in multiple adverse ways. Due to its electrical properties, airborne dust particles will regularly accumulate on the solar panels, causing a gradual loss of power production. To minimize power loss due to this dust obscuration or other damage done to the PV array, each of Horus's six triangular sectors are separately wired and connected to the power supply. Copper wiring with a thickness of 70 μm thick is used to connect the solar panels; it is thin enough to fit inside the epoxy connecting the panels to the Kevlar, therefore not adding any unnecessary thickness to the membrane. While airborne dust particles are a daily concern, global dust storms on Mars occur regularly as well, engulfing the planet and cutting the amount of solar energy reaching the Martian surface. Using data on the solar flux reduction,[12] we were able to calculate the average and minimum energy outputs during a Martian dust storm before perihelion in table 3.3, showing the reduction in electric energy produced. In order to mitigate the continuous accumulation of dust Horus will utilize an electrodynamic screen above the PV cells, maximizing the time Horus is operating at peak performance by clearing dust from the array.

Table 3.3: Horus energy output influenced by a summer global dust storm.

Location	Average Summer Dust Storm Energy Output(kWh/sol)	Minimum Summer Dust Storm Energy Output(kWh/sol)
Equator	1101.92	754.15
30°South	562.71	331.96
50°North	146.40	103.83

3.3 System 3: Electrodynamic Dust Screen System

To ensure maximum solar absorption, Horus uses an EDS to repel Martian dust particles from the surface of the solar membrane. The EDS functions by sending out electrical pulses to repel charged (and uncharged) dust particles from the PV array. Unlike other methods of dust mitigation, such as natural or mechanical, the EDS isn't compromised by the variability of the dust's electrical charge, size, or chemical composition. The particle's electrical charge, for instance, can result in a significant adhesion force between the charged particles and the PV cells,[13] while the variation in size can prevent efficient mechanical removal. In addition, the EDS system is intended to be completely self-sustainable and viable in the long term as it powers itself from the collected solar energy and is designed for minimal mechanical or electrical degradation over time.

3.3.1 Functionality

The EDS system is composed of electrodes embedded within a dielectric material, Figure 3.1. The side view (along radial direction) of the electrode layer shown in Figure 3.2 shows that the electrode layer comprises individual alternating charged electrodes separated by the dielectric medium. The electrodes utilize a three phase AC drive to generate a traveling electrical wave which steers the charged dust particles radially off the edges of the PV array.[14] This concept was first introduced as the electric curtain and was patented by Senichi Masuda in 1974.[15] The three phase system produces over 90% dust removal efficiency[14] compared to 85% efficiency of single phase AC.[16]

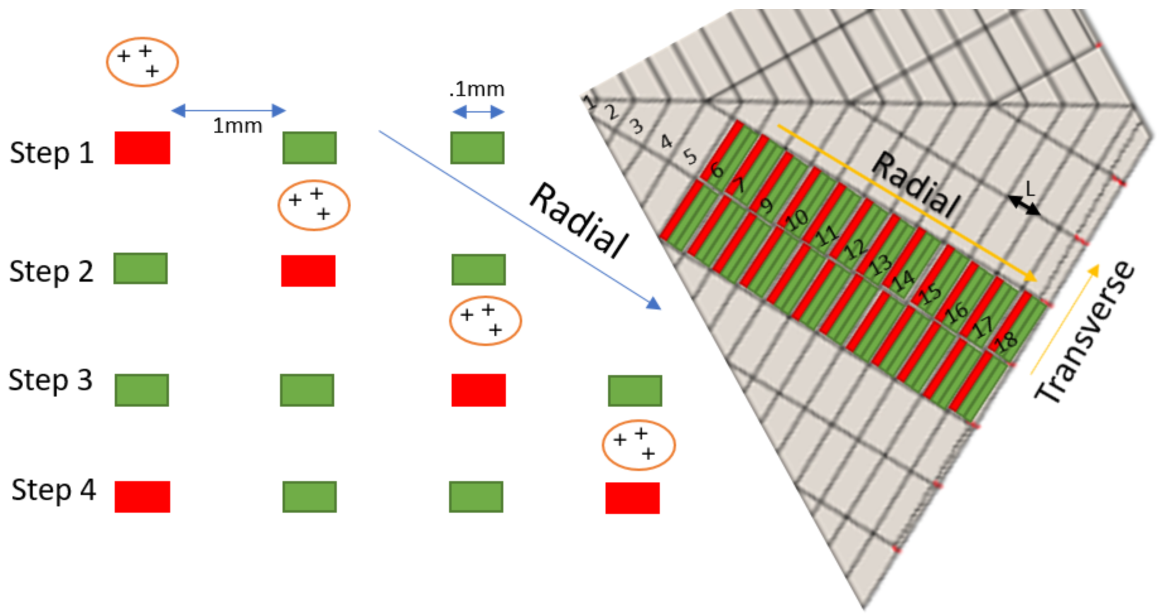

Figure 3.2: Movement of dust particle induced by traveling electric field, due to positive electrodes (green) and negative electrodes (red)

The dielectric prevents mechanical abrasion/UV damage of the electrodes (Figure 3.1). The induced dipole of neutral dust particles by the electric field produces a dielectrophoretic force, which results in the outwards radial movement of the particle similar to that of the charged particles.[14]

A 120° phase lag is selected for the three phase AC drive. This ensures that the traveling electric wave, and thus the charged dust particle, travels radially outwards (shown in Figure 3.2). Note that since $L = 1.1$ m, and electrode spacing is 1 mm, there will be roughly 1,000 electrodes on each panel, with a maximum of 18 panel or 19.8 m for the total radial distance (Figure 3.2). Assuming fully radially movement of dust particles, this translates to roughly 18,000 maximum steps to transport dust particles of one charge from the inner ring to the outer circumference. Another 18,000 steps are required to clear PV array of remaining dust particle of the other charge, along this radial direction.

An AC frequency of 10 Hz with sinusoidal signal shape optimizes performance, since low frequency with high amplitude signal gradients removes dust better.[16] 775 volts ($1550V_{p-p}$) is selected to maximize dust removal without triggering dielectric breakdown of CO_2 atmospheric gas, which is particularly susceptible in the low pressure Martian atmosphere.[17] Likewise, electrode spacing and width are 1 mm and 0.1 mm respectively (Figure 3.2), to optimize both coarse and fine dust particle removal.[14,18]

Thin Indium Tin Oxide (ITO) plates serves as the electrical connections for each of the electrodes, with dimensions 30 mm length and 0.1 mm width. These electrical connections will block a minimal area of 3,000 mm^2 for each panel, or less than 1 m for the entire PV array. The TMS320F28377S TI Single-Core Delfino Microcontroller can be used to realize power/signal control.

3.3.2 System Materials and Power Requirements

20 wt% Indium Tin Oxide (ITO) for the electrode and SCHOTT glass for the dielectric were selected. The conductivity and optical translucence of ITO makes it particularly suitable as the electrode, while 20 wt% Tin doping produced a desirable increase in energy band gap and decrease in electrical resistance.[19] ITO film thickness of 10 μm produces optimal EDS efficiency[14] without adding unnecessary weight.

SCHOTT glass, a borosilicate glass resistant to thermal shock, was selected as the dielectric for its high optical transmission, dielectric constant (≈ 6.5), and mechanical abrasion/environment resistance.[20] Glass thickness of 5μm has a breakdown voltage of 1 kV,[21] which encompasses EDS operating voltage of 750 V and avoids dielectric breakdown. Finally, the electric field strength is estimated to be 750V/100 μm or 7.5 $\frac{V}{\mu m}$ at the PV layer, which is outside the breakdown field range for GaAs.

Dust abrasion and environmental damage should overall be minimal on the EDS system. The electrodes have a long expected lifespan, as they are both shielded by the glass from the Martian environment and electrically sustainable by the PV array.

The EDS system requires 10 $\frac{W}{m^2}$,[14] or 10.61 kW for the entire array to operate. Since the solar obscuration due to dust accumulation is estimated to be .28% per day,[22] an additional 36.2 kWh of power generation lost per day due to dust accumulation is expected. To determine how often to utilize the EDS to clear the PV array, data was extrapolated from a previous NASA 2010 experiment to generously estimate a required time of 3 hours to fully clear the PV array of dust particles,[23] requiring 31.83 kWh for complete dust clear off. Comparing the cumulative energy lost from solar obscuration due to dust per day to the energy required to run the EDS, it is observed that the EDS should be used once a day to maximize energy absorption, both during the summer and the winter seasons. In the event that the EDS operation affects solar energy collection, the EDS can be utilized during dawn, to allow for and maximize dust clear off without interfering with solar collection.

4 Deployment System

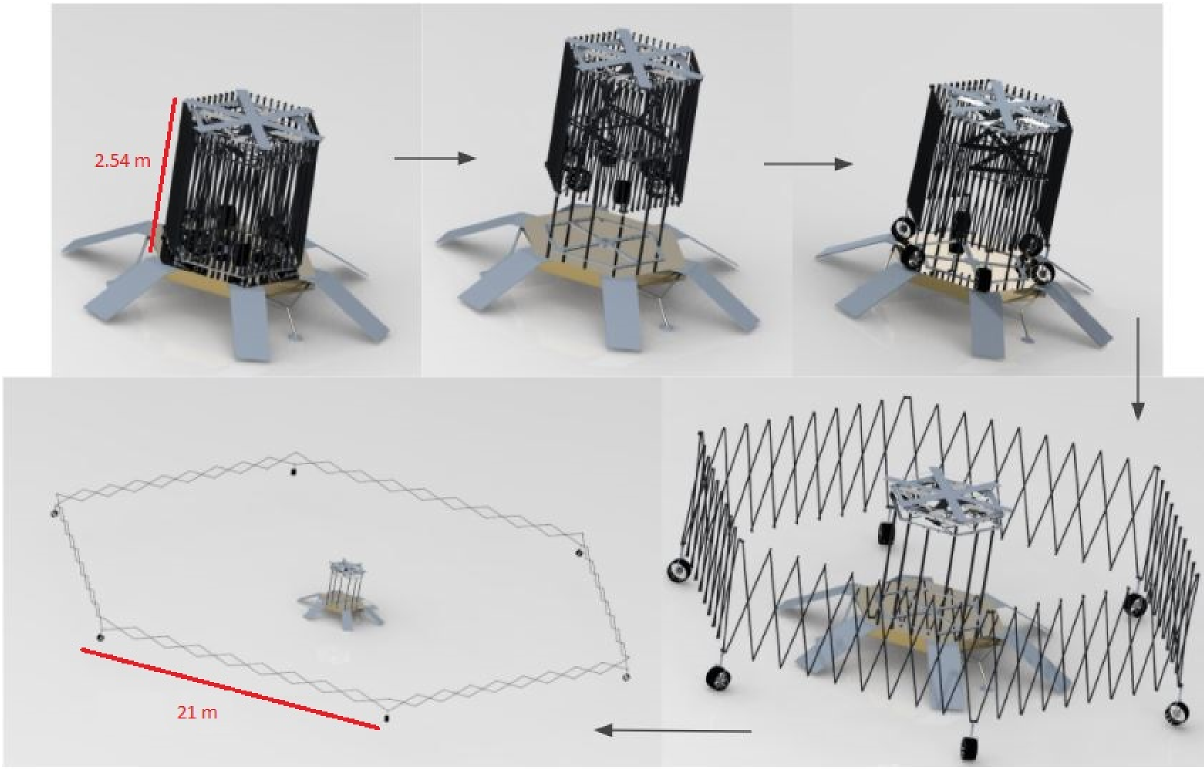

Figure 4.1: Expansion protocol, without the membrane seen on the cover page.

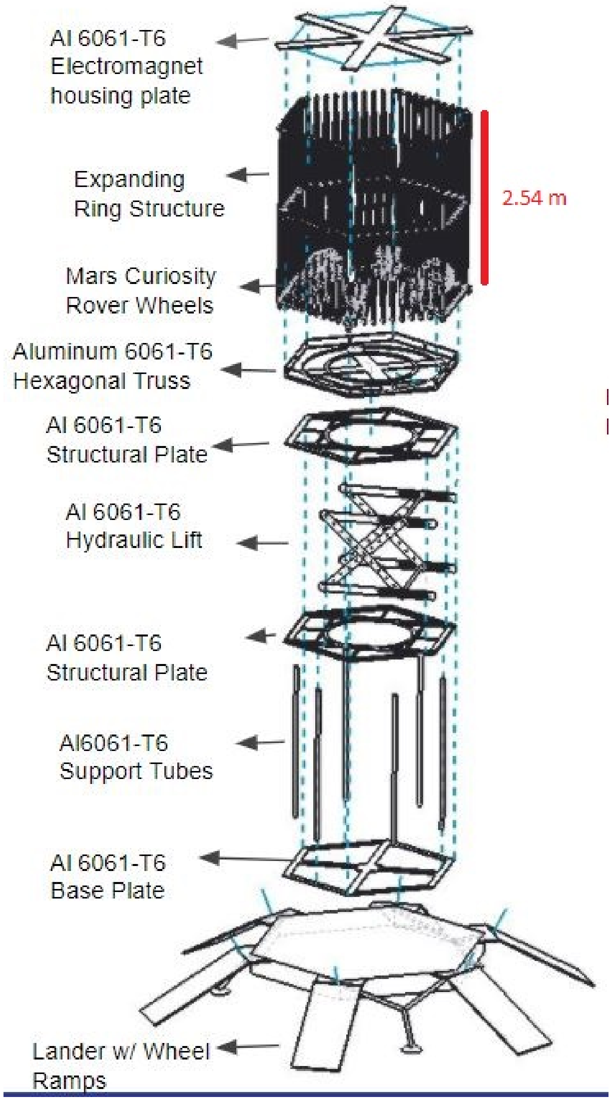

Figure 4.2: Exploded view of the deployment/support structure.

As illustrated in Figure 2.1, the Flasher requires outward radial force acting at the outer extremities of the sheet and rotation at the inner extremities of the sheet to transition from its packed state to its expanded state. This is accomplished with a hexagonally expanding ring-shaped structure, as depicted in Figure 4.1. In order to deploy, the stowed membrane and the expanding ring structure will be hydraulically lifted above the lander. Rover wheels will deploy from the expanding ring structure while it is suspended. Then, the ring structure and the folded membrane will be hydraulically lowered onto its wheels on top of the lander; the expanding ring structure will unfold the membrane to its final open surface area; the wheels will retract; and the extending hexagon structure's frame will anchor to the ground. This is described in detail in the following sections.

Figure 4.2 illustrates the entire deployment system, labeled and in an exploded view. Components of the system will be referred to as they are labeled here (although some parts attached to the expanding ring structure are not marked here). As seen in Figure 4.2 and Figure 4.1, in the packed state, the expanding ring structure rests on the lander and surrounds the remainder of the system components - which collectively form the central support column. In this packed state, the fully-folded membrane stands neatly between the central support column and the expanding ring structure.

4.1 Membrane Attachment Points

Horus's membrane is at all times suspended between the expanding ring structure and the hexagonal truss. The interior of the membrane attaches to the hexagonal truss component - which rotates about the support plate it sits on via bearings, facilitating the rotation of the center of the membrane during deployment. The Kevlar layer wraps around the upper beam of the hexagonal truss, as shown in Figure 4.3, and is stitched to itself. The exterior of the membrane is attached to the expanding ring structure as a boat's sail is attached to its mast. It is necessary to make cuts in the membrane at certain locations to ensure that the outer attachment points between the expanding ring structure and the Kevlar align properly.

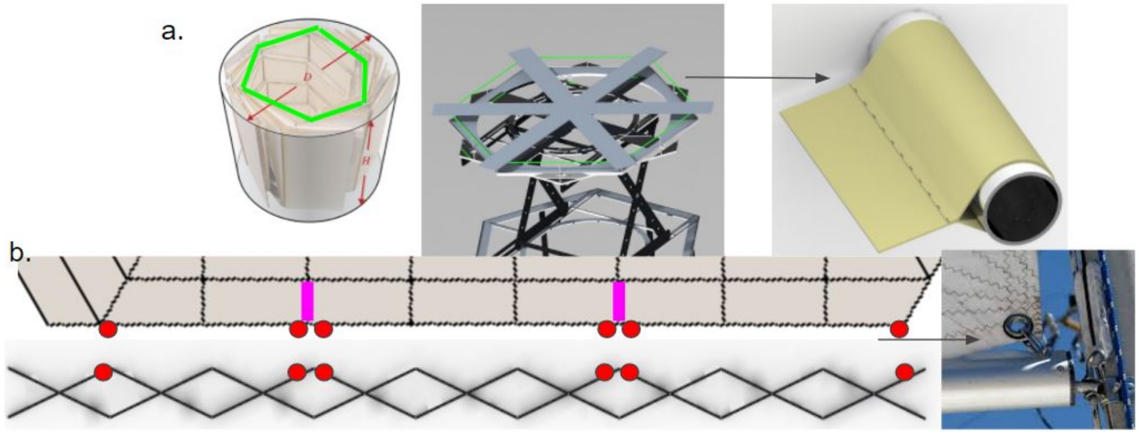

Figure 4.3: (a) At its interior opening (green), the Kevlar layer wraps around the green-painted bar of the Al6061-T6 hexagonal truss. (b) At its perimeter, the Kevlar layer attaches to the expanding ring structure as a sail would its mast. Red dots represent corresponding attachment points between the expanding ring structure and the membrane. Pink lines represent cuts.

4.2 Phase 1: Elevating the Expanding Ring Structure and Folded Membrane

Starting in its packed state, Horus's expanding ring structure sits flat on the lander. The membrane is suspended between the top of the expanding ring structure and the hexagonal truss - which sits on top of the compact-state hydraulic lift and a lightweight chassis consisting of the base plate, support tubes, and lower structural plate. The first step of Horus's deployment protocol is to lift the expanding ring structure so that the wheels, which are stowed inside the payload, may fold down into place. This is executed by a hydraulic lift mechanism. The hydraulic lift raises the hexagonal support truss a distance of up to one meter in height, bringing with it the inner attachment of the membrane. An electromagnet housing plate is fixed on the top of the hexagonal support truss, as seen in Figures 4.2 and 4.4. 400 kg capacity electromagnets sit at each of the six ends of the housing plate, and their oppositely charged counterparts are fixed to aluminum brackets on the six upper corners of the expanding ring structure. When lifting protocol is called, the electromagnets are set to their on-state and will draw 33 W of power (6.6 Wh over a projected two minutes of engagement).[24] This provides a temporary fixed connection between the expanding ring structure and the hexagonal truss, allowing for the hydraulic lift to elevate the expanding ring structure as well. A 1,000 kg capacity hydraulic lift can bear the load of the expanding ring structure and the membrane, weighing 950 kg on Earth, and can do so with a safety factor of 3.34 on Mars. Using data/specifications from Global Industrial for a commercial hydraulic elevator, raising the array to its proper expanding height will require approximately 3.1 Wh of energy. While hydraulic propulsion is complicated by the need to travel through the vacuum space, it is still a well-established space-flight technology, as hydraulic systems are necessary for guiding the space shuttle thrusters' vector control systems under very high forces.[25]

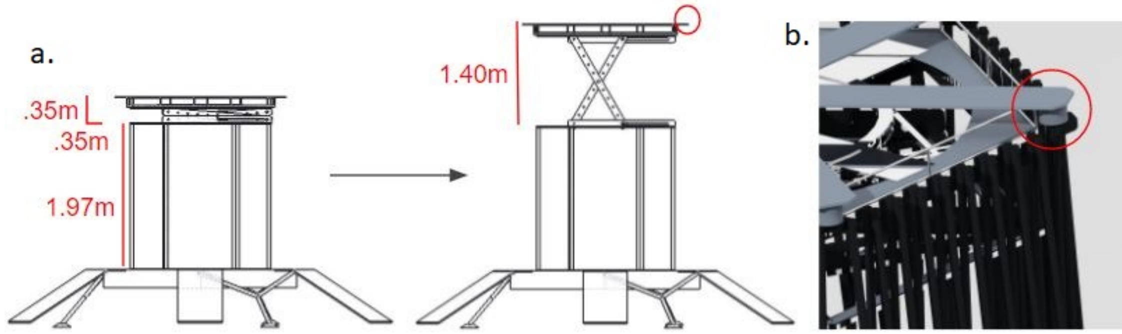

Figure 4.4: (a.) The hydraulic lift elevates, bringing the membrane and the expanding ring structure with it. (b.) Electromagnets temporarily fix the expanding ring structure to the hexagonal truss, so that they are lifted together.

4.3 Phase 2: Wheel Deployment

Once the expanding ring structure is suspended, six wheels - one at each corner of the expanding ring structure - are deployed. The wheels are lowered as shown in Figure 4.5 (cite product?). Once the wheels are locked in place, the hydraulic lift lowers the expanding ring structure, now on wheels, down to the lander (Figure 4.1). Scaled-down Mars Curiosity Rover wheels were chosen for durability, low mass, and technological readiness. These large, 40 cm diameter wheels are the Horus's primary means of handling the rough Martian terrain. Should any truly difficult obstacle be encountered during deployment, the rotary actuators are capable of retracting the wheel at any time.

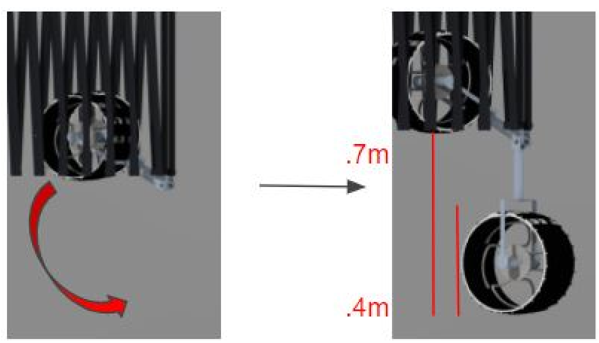

Figure 4.5: Wheels deploy angularly, driven by a rotary actuator. Wheel width = 23.6 cm.

4.4 Phase 3: Radial Expansion

Once the expanding ring structure is on wheels, radial expansion can commence. Over the course of expansion, each of the scissor mechanisms that form the sides of the ring extend from roughly 1.5 m to 21 m long, as shown in Figure 4.1. This expansion is resisted by a tensile force applied by the membrane in the inward radial direction; the magnitude of this force increases as the ring expands. A crude estimate of this tension was estimated for Earth conditions as 10 kN over the fully expanded ring, or 1.7 kN per side of the ring by modifying the cable equation,[26]

$$T = WL/(8h)$$

where W is the weight of the membrane, L is the average radius of the Horus, and h is the maximum allowed sag in the membrane. This tension force will cause an equivalent compressive load of 1.7 kN to develop in each of the sides of the expanding ring. A series of electric winches are placed at the six top corners of the expanding ring structure (Figure 4.6) to drive the expansion of the ring against this compressive load. As the winches contract their respective cables, the expanding ring is forced open. For reference, the Ironton double line electric winch can provide 2 kN of cable tension, weighs 10 kg, and requires 125 W of power.[27] The speed of the wheels over the ground is set to match the top speed of the Curiosity rover, 4 cm/s. At this speed, the third phase of deployment takes 9 minutes, during which the winches consume 113 Wh of energy. The beams in the expanding ring have an I-beam cross section to mitigate bending of the scissor mechanisms in the radial direction. Each of the I-beams has a 5 cm flange length, 4 mm flange thickness, 8 cm web length, and 8 mm web thickness. Beryllium S-200F was chosen as the material for the beams due to its high strength to weight ratio, low thermal expansion coefficient, and history of use in aerospace structures.[28] Al6061-T6 was chosen for the pins in the expanding ring to minimize friction between the beryllium beams.

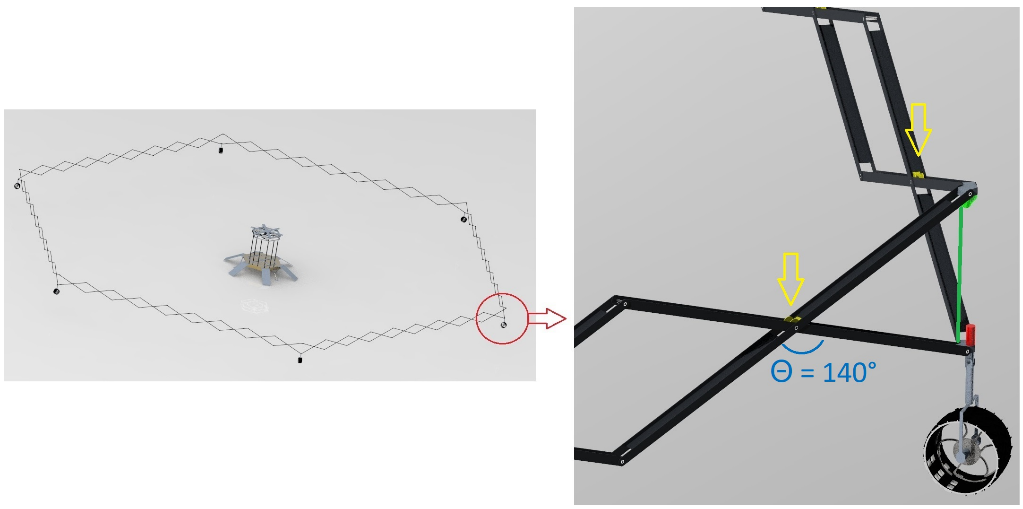

Figure 4.6: Close up view of a corner of the expanding ring. The electric winch and its cable are shown in green, folding brackets are shown in yellow, and the anchor mechanism is shown in red.

4.5 Phase 4: Anchoring

With the ring fully expanded, three processes complete the deployment of the Horus. First, when the beams in the support structure reach an angle of about $\theta = 140°$, a series of folding brackets[33] located on the beams (see Figure 4.6) lock into place, preventing any further expansion or contraction of the expanding ring. Next, the wheels on the corners of the expanding ring fold back, resting the expanding ring structure on the ground. Finally, units located at the corners of the ring fire anchoring projectiles into the ground. Cables attached to the projectiles are then tightened with an electric winch. These anchoring units, estimated to weigh 10 kg apiece, were originally developed to facilitate asteroid landings and function for a wide range of terrain, from hard rock to snow.[29] Anchoring the Horus serves primarily to counteract lifting forces produced by heavy winds, but also prevents horizontal displacement of the expanding ring structure.

5 Structural Performance

5.1 Structure Validation

5.1.1 Expanding Ring Buckling Analysis

The 21 m long sides of the fully expanded ring are the structural elements most susceptible to bending and buckling. These elements were simulated using Creo Parametric 4.0 under earth loading conditions to verify 1) that the stresses imposed by the Kevlar sheet do not exceed the yield stress of beryllium and 2) that the compressive load on the sides of the ring does not result in buckling. The Young's modulus of beryllium used in the simulation was 278 GPa, and its yield strength is 345 MPa.[30] Figure 5.1 shows the deformations on one side of the ring when the compressive loads are applied and the radial loads of the Kevlar sheet are applied at the attachment points discussed in section 4.1. The safety factor of the bucking analysis done using this distribution of forces was 2, meaning that the structure can handle approximately double the applied forces before buckling occurs.

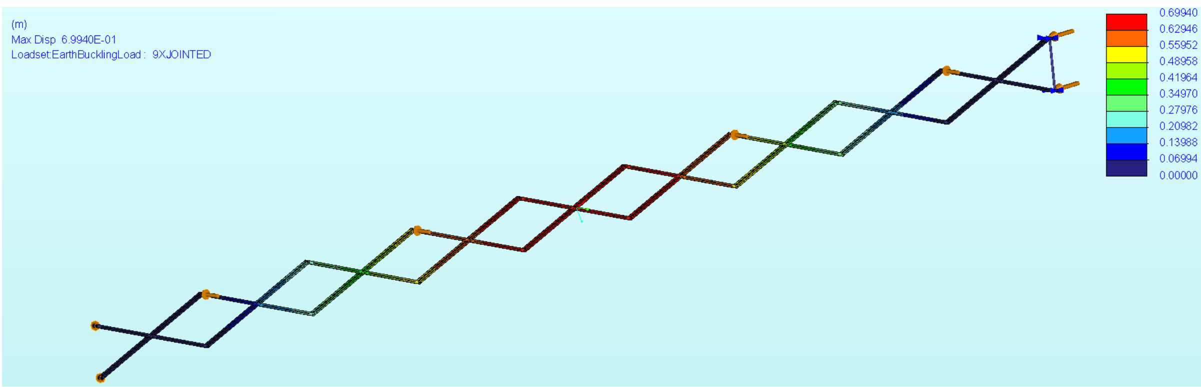

Figure 5.1: Deformations of the outer ring structure. The scale on the right measures deformation of the structure in meters.

5.1.2 Central Support Stress Analysis

The central support column is comprised of Aluminum 6061-T6 to be strong, lightweight, and corrosion-resistant. Static analysis indicates the highest stress concentrations to appear at two free corners unaligned with the hydraulic lift. Maximum stress in these locations reaches 155 MPa - only about half of Al6061-T6's yield stress. Here, deflection reaches up to 1.5 cm with a load of 1,500 kg on Earth; realistically the structure will be supporting closer to 1,000 kg (the weight of the membrane and expanding ring structure, minus the weight of the central support column), and under Martian gravity.

5.2 Lift Determination of Membrane Using Lifting Line Theory

A primary consideration for the Horus is lift force generated during Martian dust storms. Because the membrane has a large surface area subject to wind, determining the maximum lift force was necessary to ensure that the array would not fly away or flap too violently. However, the calculated Reynolds number of the Horus is roughly 1.1 million, assuming 50 $\frac{m}{s}$ surface winds and the width of Horus. This made simulations impractical, due to the increase in resolution needed and corresponding increase in simulation time.

Alternatively, Lifting Line Theory was applied with an additional 20% error factor to determine a rough-estimated maximum lift force of approximately 5674 N (lift coefficient $\approx .3$) for surface winds parallel to the ground ($\alpha = 0$). This error factor was included because Lifting Line Theory is intended for high aspect ratio (the Horus's is 1.1, which is low), and to compensate for additional complex effects which could increase the lift coefficient, including the aeroelasticity of the large sheet and the increased pressure differential arising from constricted airflow underneath the sheet (due to ground boundary layer and outer support ring). To address concerns of lift, we used an anchoring mechanism discussed in Section 4.5.

5.3 Membrane Thermal Cycling and Thermal Shock

Large daily temperature fluctuations of 125 degrees C will cause additional stresses within the membrane due to differential thermal expansion of different materials. Because Kevlar is the thickest and stiffest material in our membrane, it dictates the expansion of other materials. Therefore, the thermal stresses in different materials can be estimated as

$$\sigma_{\text{thermal}} = E(\alpha_{\text{kevlar}} - \alpha)\Delta T,$$

where σ_{thermal} is thermal stress, E is the Young's modulus of material, α is the material's thermal expansion coefficient (TEC), α_{kevlar} is the TEC of Kevlar, and $\Delta T = 125K$ is the maximum change in daily temperature on Mars. Table 5.1 displays thermal stresses for different materials. Thermal shock, or stress related to temperature gradient of the material, is not as consequential, as Kevlar, Supreme 10HT, SCHOTT glass, and SiO_2 layers all have excellent thermal shock resistance, while ITO is highly conductive so thermal shock is unlikely to be an issue. GaAs have also been successfully utilized in previous Martian exploration rovers. Finally, we consider thermal performance of the material, or the effect of temperature on the material strength, and all of the material used retains its strength even at low temperature.

Table 5.1: Maximum Thermal Expansion Coefficient and Thermal Cycling

Material	TEC $10^{-6}(K^{-1})$	Young's Modulus (GPa)	Thermal Stress, Δ T = 125K (MPa)
Kevlar KM2	2.7	112	0
Supreme 10HT	47	3.45	-19.1
$GaAs$	.573	85.5	-32.4
SIO_2	.65	7	17.9
ITO	.00454 to 6.374	116	2.7 to -53.3
SCHOTT Glass	7.2	.0729	-.041

5.4 Membrane Structural Validation and Thermal Cycling

In order to verify the integrity of membrane, we tested whether any of the materials could yield or fracture under expected loading conditions. We have determined principal stresses σ_p and the total deflection with the CREO Simulate software for 4 different scenarios. Simulation 1 concerns with deployment on Earth, while simulations 2, 3, and 4 concerns with Martian atmosphere and conditions.

The simulations were performed with the same constraint conditions shown in Figure 5.2 but different loadings: Simulation 1 – Earth's gravity (-$\hat{z}$) without wind, Simulation 2 – Martian gravity ($-\hat{z}$) without wind, Simulation 3 – Martian gravity ($-\hat{z}$) and lift force ($\hat{z}$) from 50 $\frac{m}{s}$ surface winds for the

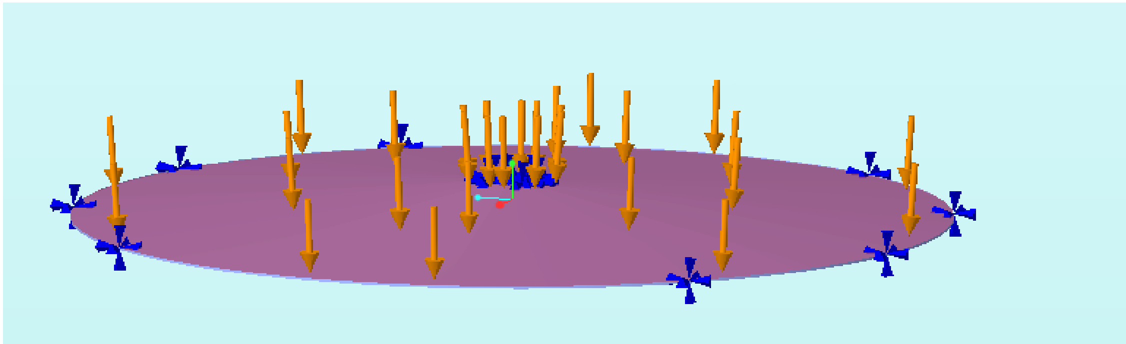

Figure 5.2: CREO Simulate of the membrane. Membrane is fixed at the blue points on inner and outer radius. Orange arrows indicate pressure loads due to wind and gravity.

zero angle of attack, Simulation 4 – Martian gravity (-$\hat{z}$) and the wind pressure distribution of 27 Pa (-$\hat{z}$).

Note that simulation 4 arise from the extreme scenario where the winds of 50 $\frac{m}{s}$ push the top of PV array downwards, resulting in a maximum pressure impact of 27 Pa (calculated through Bernoulli's equation). Results are tabulated in Table 5.2, as well as corresponding material yield strength σ_y and tensile fracture strength σ_f in Table 5.3.

The primary failure mode concerned is yielding ($\sigma \geq \sigma_y$) or fracture ($\sigma \geq \sigma_f$). Simulation 1, 2, and 3 indicates that the membrane can be fully deployed on Earth and Mars, as well as endure Martian surface winds of 50 $\frac{m}{s}$, without triggering the failure mode (See Tables 5.3 5.2). Accounting for MTS (maximum thermal stress, Table 5.1) in simulations 2 and 3, the failure mode is still not reached. Unfortunately yield stress values are not available for all of the materials used, but the stresses appear to be suitably low for these materials ($\sigma < \sigma_y$). For simulation 4 (extreme condition) plus MTS, the epoxy layer has likely reached yield and approaches fracture, while GaAs begins to approach yield (Tables 5.2, 5.3). While its difficult to definitely address failure mode due to a lack of verifiable material information, it appears that only the extreme scenario (Sim 4) is of concern due to the epoxy layer. However, stronger and more suitable epoxy are/will likely be available, so this is unlikely to be a limiting factor in the overall design.

Table 5.2: CREO Stress and Displacement Simulations with Different Loading Conditions

Material	Sim1, $\sigma_{p_{max}}$ (MPa)	Sim2, $\sigma_{p_{max}}$	Sim3, $\sigma_{p_{max}}$ (MPa)	Sim4, $\sigma_{p_{max}}$ (MPa)
Kevlar KM2	25.57	9.6	12.74	134
Supreme 10HT	6.3	2.385	3.12	35.1
$GaAs$	13.33	5.27	6.98	73.9
SIO_2	11.78	4.332	5.9	29
ITO	18.9	7.117	9.38	35.94
SCHOTT Glass	11.56	4.37	5.88	21.71
Membrane Deflection	8.89 mm	3.51 mm	5.08 mm	48.51 mm

Table 5.3: Yield Stress, Tensile Stress

Material	Yield Stress (MPa)	Tensile Stress
Kevlar KM2	1240	3600
Supreme 10HT	currently unknown	60
GaAs	100-200	currently unknown
SIO_2	45-155	310
ITO	currently unknown	150
SCHOTT Glass	currently unknown	120-200

5.4.1 Sound and Axial Load During Lift Off

Horus will first need to get into orbit before it can do any work so it is important that it can withstand the loadings and acoustic pressure fields generated by a rocket during liftoff. As per the challenge's guidelines, Horus was tested to insure that it could survive axial loadings of at least 5 g's, lateral loadings of at least 2 g's and the pressure field generated by 145 dB of Overall Sound Pressure Level (OASPL). The 145 dB convert to a pressure of 356 Pa. All of Horus's components were subjected to each individual loading and an additional simulation where all 3 loadings act on the structures at the same time. Results were favorable. Maximum Principal stresses peaked at 11.8 MPa while the lowest Yield Stress corresponded to the Supreme 10HT Epoxy with a value of 60 MPa. One concern was that the outer ring structure would deflect inwards and strike the PV membrane. Simulation results showed that the maximum deflection for the outer ring structure was on the order of 0.052 mm thus ensuring that no interaction would take place between the membrane and outer ring structure.

5.5 Optical Transmission of System

A primary concern with the Horus's EDS system was the possibility of interference with the PV layer's ability to absorb photons. Using both the Fresnel Equations and the Transfer Matrix Method, the total optical transmission for normal incidence conditions with perpendicular light was determined (EDS system and PV Array) to be between 90-95% for the entire system from 100-900 nm.[31] Since the band gap of GaAs is roughly 1.4 eV, photon energy should be insufficient past 900-1000 nm, as photon energy decrease with increasing wavelength. As such, the steep drop in optical transmission past roughly 900 nm isn't of significant concern for the Horus.

6 Conclusion

The Horus solar array combines existing technology with new ideas, and is the large PV array NASA needs for its future space endeavors on Mars. With its Gallium Arsenide solar panels, the PV array can produce an average of 1294 kWh daily along the Martian equator. Adding the estimated masses of the membrane, the expanding ring structure, and the central structural elements, Horus has a total mass of 1390 kg, meeting the mass constraint of 1500 kg. With a robust electrodynamic dust shield, the Horus can clear dust that has accumulated on its panels and ensure maximal solar absorption. Horus requires no external assistance upon landing to properly deploy. Once the Horus has landed on Mars it takes care of itself, so NASA and their astronauts can spend less time worrying about surviving on Mars and more time learning about it.

References

[1] Zirbel SA, Lang RJ, Thomson MW, et al. "Accommodating Thickness in Origami-Based Deployable Arrays". Journal of Mechanical Design. Vol 135, no.11, 2012. http://mechanicaldesign.asmedigitalcollection.asme.org/article.aspx?articleid=1737156

[2] Guest, S.D., and Pellegrino, S. (1992). "Inextensional Wrapping of Flat Membranes." First International Conference on Structural Morphology, Montpellier, R. Motro and T. Wester, eds., 7-11 September, 203-215. http://www2.eng.cam.ac.uk/~sdg/preprint/Wrapping.pdf

[3] R Destefanis, E Amerio, M Briccarello, M Belluco, M Faraud, E Tracino. "Space environment characterisation of Kevlar: good for bullets, debris and radiation too" Universal Journal of Aeronautical & Aerospace Sciences 2, 80-113

[4] Da Silva, Lucas F. M. , and R D Adams. "Measurement of the mechanical properties of structural adhesives in tension and shear over a wide range of temperatures". , Universidade do Porto, Universidade de Oporto, 2004, paginas.fe.up.pt/~lucas/daSilva_JAST_2005.pdf.

[5] Dupont. Kevlar Aramid Fiber Techbucak Guide. Kevlar Aramid Fiber Technical Guide, from www.dupont.com/content/dam/dupont/products-and-services/fabrics-fibers-and-nonwovens/fibers/documents/Kevlar_Technical_Guide.pdf.

[6] Chen, Ming, et al. "Mechanical Properties of Kevlar KM2 Single Fiber." Journal of Engineering Materials and Technology, 2005, from www.researchgate.net/profile/Ming_Cheng12/publication/249505554_Mechanical_Properties_of_KevlarR_KM2_Single_Fiber/links/541894b20cf203f155adb1f8/Mechanical-Properties-of-KevlarR-KM2-Single-Fiber.pdf.

[7] Landis, Kerslake, Jenkins, and Sheiman. "Mars Solar Power." Second International Energy Conversion Engineering Conference sponsored by the American Institute of Aeronautics and Astronautics. Providence, Rhode Island, 2004, from https://ntrs.nasa.gov/archive/nasa/casi.ntrs.nasa.gov/20040191326.pdf

[8] Kumar, Suresh, and Nagaraju. "Measurement and comparison of AC parameters of Silicon (BSR and BSFR) and gallium arsenide(GaAs/Ge) solar cells used in space applications." Solar Energy Materials and Solar Cells, Volume 60, Issue 2. 15 January 2000, 155-166, from http://www.sciencedirect.com/science/article/pii/S092702489900080X

[9] Frazier, Sarah. "Real Martians: How to Protect Astronauts from Space Radiation on Mars." NASA's Goddard Space Flight Center, 2017, from https://www.nasa.gov/feature/goddard/real-martians-how-to-protect-astronauts-from-space-radiation-on-mars

[10] National Renewable Energy Laboratory. "Best Research Cell Efficiencies". NREL, from https://www.nrel.gov/pv/assets/images/efficiency-chart.png

[11] Jet Propulsion Laboratory."Extreme Planet Takes its Toll". NASA, from https://mars.nasa.gov/mer/spotlight/20070612.html

[12] Big Idea Challenge."Max Horizontal Solar Fluxes". NASA, from http://i1.wp.com/bigidea.nianet.org/wp-content/uploads/2017/10/Mars-Solar-Flux2.jpg

[13] Landis, Geoffrey. "Mars Dust Removal Technology." Energy Conversion Engineering Conference, 1997. IECEC-97., Proceedings of the 32nd Intersociety, from http://ieeexplore.ieee.org/stamp/stamp.jsp?arnumber=659288

[14] Mazumder, M. K., et al. "Self-Cleaning Transparent Dust Shields for Protecting Solar Panels and Other Devices." Particulate Science and Technology, vol. 25, no. 1, 2007, pp. 5âĂŞ20., doi:10.1080/02726350601146341.

[15] Masuda, Senichi. "Booth for Electrostatic Powder Painting with Contact Type Electric Field Curtain." 2 April 1974.

[16] Biris, A.s., et al. "Electrodynamic Removal of Contaminant Particles and Its Applications." Conference Record of the 2004 IEEE Industry Applications Conference, 2004. 39th IAS Annual Meeting.

[17] Calle, C.i., et al. "Active Dust Control and Mitigation Technology for Lunar and Martian Exploration." Acta Astronautica, vol. 69, no. 11-12, 2011, pp. 1082-1088.

[18] Johnson, C.e., et al. "Effect of Particle Size Distribution on the Performance of Electrodynamic Screens." Fourtieth IAS Annual Meeting. Conference Record of the 2005 Industry Applications Conference, 2005., doi:10.1109/ias.2005.1518330.

[19] Thirumoorthi, M., and J. Thomas Joseph Prakash. "Structure, Optical and Electrical Properties of Indium Tin Oxide Ultra Thin Films Prepared by Jet Nebulizer Spray Pyrolysis Technique." Journal of Asian Ceramic Societies, vol. 4, no. 1, 2016, p. 124-132.

[20] SCHOTT. "Ultra-Thin Glass.". SCHOTT Press Releases as RSS, from `www.us.schott.com/advanced_optics/english/products/wafers-and-thin-glass/glass-wafer-and-substrates/ultra-thin-glass/index.html#block363641`

[21] Skanavi, G. I., Fizika Dielektrikov; Oblast Silnykh Polei. "Physics of Dielectrics; Strong Fields". Gos. Izd. Fiz. Mat. Nauk (State Publ. Housefor Phys. and Math. Scis.), Moscow, 1958.

[22] Mazumder, M. K., et al. "Solar Panel Obscuration in the Dusty Atmosphere of Mars."

[23] Calle, Carlos, et al. "Electrodynamic Dust Shield for Solar Panels on Mars." 2004.

[24] BuyMagnets.com. "Round Electromagnets, Flat-Faced." `https://buymagnets.com/product-pdfs/BDE-4032-12.pdf`

[25] Parikh, Darshak. "Hydraulics in Space". Engineering Clicks, 13 May 2017. `https://www.engineeringclicks.com/hydraulics-in-space`

[26] `https://www.engineeringtoolbox.com/cable-loads-d_1816.html`

[27] Ironton. "Ironton Double Line Electric winch - 220-Lb. Single Line/440-Lb. Double Line LiftCapacity." Northern Tools `www.northerntool.com/shop/tools/product_200660034_200660034`

[28] Jakubke, Hans-Dieter; Jeschkeit, Hans, eds. (1994). Concise Encyclopedia Chemistry. trans. rev. Eagleson, Mary. Berlin: Walter de Gruyter.

[29] Ghavimi, R A, et al. "Autonomous Landing and Smart Anchoring for In-Situ Exploration of Small Bodies." Artificial Intelligence, Robotics and Automation in Space, Proceedings of the Fifth International Symposium, 1 June 1999, pp. 609-611., adsabs.harvard.edu/abs/1999ESASP.440..609G.

[30] `https://materion.com/-/media/files/beryllium/beryllium-materials/mb-001designingandfabricatingberyllium.pdf`

[31] Lvovsky, Alexander I.. Fresnel Equations. In Encyclopedia of Optical Engineering. Taylor and Francis: New York, Published online: 27 Feb 2013; 1-6. http://iqst.ca/quantech/pubs/2013/fresnel-eoe.pdf

[32] Global Industrial. "Bishamon OPTIMUS Lift2K Power Scissor Lift Table 48x28 2000 Lb. Cap. Hand Control L2K-2848". https://www.globalindustrial.com/p/material-handling/lift-tables/stationary/bishamon-li-2k-power-scissor-li-table-48-l-x-28-w-2000-lb-capacity?infoParam.campaignId=T9F&gclid=EAIaIQobChMImqHN3biq2QIVkrrACh2ykQemEAYYCSABEgJydvD_BwE

[33] locksonline.com. "Steel Folding Bracket for Tables and Benches." https://www.locksonline.com/Steel-Folding-Bracket-for-Tables-and-Benches-for-38mm-x-38mm-Legs-1385.html

[34] Hibbeler, R. C. "Mechanics of Materials." Pearson, 2014.

[35] NASA. "Home, Space Home". March 31, 2001, from https://science.nasa.gov/science-news/science-at-nasa/2001/ast14mar_1